esa SP - 359
March 1993
Volume I

Proceedings of the First ERS-1 Symposium

SPACE AT THE SERVICE OF OUR ENVIRONMENT

4 - 6 November 1992
Cannes, France

european space agency / agence spatiale européenne
8-10, rue Mario-Nikis, 75738 Paris Cedex 15, France

PRELIMINARY RESULTS OF THE EXPERIMENT I-7

C. Cafforio[1], G. De Carolis[2], F. Mattia[2], A. Moccia[3], S. Ponte[3], F. Posa[1,4], V.D. Schena[5], R. Sergi[5], P. Smacchia[6], V. Sozzi[4], S. Vetrella[3]

[1] Politecnico di Bari; [2] GNCB-CNR, Bari; [3] Università degli Studi Federico II, Napoli; [4] Dipartimento di Fisica, Bari; [5] CORISTA, Napoli; [6] ITIS-CNR, Matera.

ABSTRACT

This paper describes the preliminary results related to the ERS-1 AMI image mode data analysis carried out in the framework of the Experiment I-7. The SAR data have been acquired during the October 23rd 1991 night pass over the Salento Peninsula and the June 21st and July 7th 1992 day passes over the Matera area in Southern Italy. In this experimental phase, the main objectives are the SAR Image Quality Evaluation and Calibration. To accomplish this, two Active Radar Calibrators and several trihedral corner reflectors have been deployed on both sites. The Data Sets are extracted from SLC products provided by the SAR VMP installed at the Earthnet Programme Office, Frascati, and from PRI products processed at the I-PAF, Matera, Italy; in addition, a preliminary comparison with the SAR ω-κ Processor, available within our group, is presented.

Keywords: ERS-1, AMI Image mode, Data quality analysis, Radiometric calibration.

1. DATA QUALITY ANALYSIS

1.1 Background

In order to test the Verification Mode Processor (VMP), the PRI I-PAF processor performances as well as those of the ω-κ processor (Ref. 1) in terms of their spatial and energy focusing properties, a number of quality tests has been performed on each product. The measurements have been carried out on trihedral corner reflectors and ARCs previously deployed on the sites imaged by the ERS-1 SAR sensor. The point targets were identified by visual inspection of the images, and their geographical location was verified by using Istituto Geografico Militare Italiano (IGMI) maps and GPS recorded data.

The Image Quality Analysis (IQA) tests provided evaluations of the one-dimensional spatial resolutions, and energy focusing measurements, such as the Integrated Sidelobe Ratio (ISLR) and the Peak Sidelobe Ratio (PSLR) (Ref. 2). The resolutions are obtained by computing the number of samples which are contained in the 3dB region with respect to the peak value of the point target mainlobe response, oversampled by using FFT techniques (Ref. 3).

The Earth curvature effect has been taken into account in the evaluation of the ground range (ρ_{gr}) and azimuth (ρ_{az}) resolutions, leading to the geometry depicted in Fig. 1.

The corresponding equations for the 1D resolutions are as follows (Ref. 4), (Ref. 5):

$$\rho_{gr} = (N_{3R} - 1)\left[(R\delta\alpha)^2 + \left(\frac{c}{2 f_s M_0} \right)^2 \right]^{1/2}$$

$$\rho_{az} = (N_{3A} - 1) R_e \cos^{-1}\left[\sin^2\beta + \cos^2\beta \cos\left(\frac{\delta\vartheta}{M_0} \right) \right]$$

Geometry:

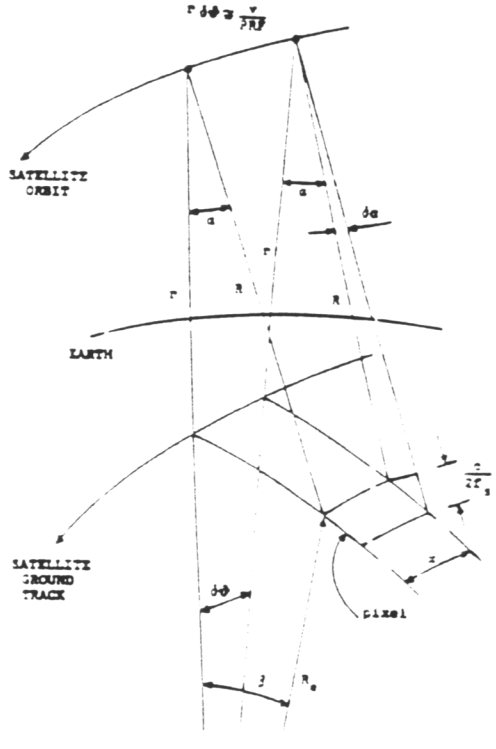

Fig. 1. Spaceborne SAR geometry.

where:

$$\delta\alpha = \frac{c\, r\cos\alpha - R}{2 f_s M_0 R\, r \sin\alpha}$$

$$\beta = \sin^{-1}\left(\frac{R}{R_e} \sin\alpha \right)$$

and α is the off-nadir angle, R_e is the local Earth radius according to the Goddard Earth Model 6 (GEM6), r is the modulus of the satellite position vector in the inertial reference frame, N_{3R} and N_{3A} are the number of samples inside the range and azimuth 3dB lobes, respectively, $\delta\alpha$ is the off-nadir angle difference between two adjacent range samples.

Proceedings First ERS-1 Symposium - Space at the Service of our Environment, Cannes, France, 4 - 6 November 1992
ESA SP-359 (March 1993)

β is the geocentric angle between the satellite and the range sample, $\delta\theta$ is the satellite true anomaly step corresponding to 1/PRF and M_0 is the oversampling factor. Assuming a Keplerian orbit, the range R and the satellite velocity v are given, respectively, by:

$$R = a\cos\alpha - \left(R_e^2 - a^2\sin^2\alpha\right)^{1/2}$$

$$v = \left[\frac{\mu_e}{a}\left(\frac{2a}{r} - 1\right)\right]^{1/2}$$

where μ_e is the Earth gravitational constant, and a is the orbit semi-major axis. The computation of ρ_{az} takes into account the beam-to-spacecraft velocity ratio proposed in (Ref. 4), but if the additional effect of the off-nadir angle is negligible, i.e. if $\beta \ll 1$ and $\frac{v}{r\,PRF} \ll 1$, then a good approximation for ρ_{az} is given by (Ref. 5):

$$\rho_{az} = (N_{3A} - 1)\left(\frac{v\,R_e}{M_0\,r\,PRF}\right)$$

As for the energy focusing tests, in the oversampled range and azimuth lines containing the point target position, and for each cut box, an evaluation of range and azimuth ISLR and PSLR has been carried out, having assumed the mainlobe zone as 2ρ-extended with respect to the peak value, and the sidelobe zone as 10ρ-extended outside the mainlobe zone (Ref. 2). The nominal values for PSLR and ISLR are, respectively, -13.2 dB and about -9 dB, while the nominal values of slant range, ground range and azimuth resolutions, derived by the system parameters of Table 1, are 8.51 m, 21.8 m and 4.40 m. These values have been computed assuming a sinc-like impulse response function, and taking into account the orbital corrections evaluated in (Ref. 4), (Ref. 6).

Table 1: Basic ERS-1 system parameters.

Wavelength	5.65 cm
Frequency	5.3 GHz (C-band)
Flight altitude	780 km
Look angle (near range)	19.376°
First pixel range time	5545.521 ms
Chirp bandwidth	15.5 MHz
Range sampling frequency	19 MHz
PRF	1679.902 Hz
3dB azimuth beamwidth	0.288°

1.2 VMP data quality analysis

For each point target, a square box of 32-by-32 complex pixels has been cut around the point position: this "information box" is the input of the Corner Reflector ANalysis (CRAN) routines developed by the group. The analyzed VMP product is a Single Look Complex (SLC) image, processed not at baseband, but with an unchanged residual Doppler centroid. A set of image characteristics is listed in Table 2, as extracted from the Main Product Header (MPH) record of the product (Ref. 7).

The VMP image has been obtained by processing raw data acquired on June 21, 1992 (orbit 4876; frame 2781; day pass). When the ERS-1 AMI instrument covered Matera test-site, six trihedral corner reflectors and two Active Radar Calibrators were deployed over a homogeneous background in a relatively flat zone. Table 1 reports a set of basic ERS-1 system parameters used for extracting the image quality measures described below, while in Figs 2a, 2b, the range and azimuth spectra of the VMP data over the calibrators zone are plotted.

Table 2: VMP product specifications for Matera data.

Date of processing	July 10th, 1992
Type of product	Single Look Complex
I/Q Data Format	16 bits/sample
Slant range pixel spacing	7.905 m
Azimuth pixel spacing	3.980 m
Residual Doppler centroid	399 Hz
Geographical location	40.636°N, 16.403° W (centre pixel)
Processing	Processed with Extracted Chirp
Look Detection	Power detected & summed

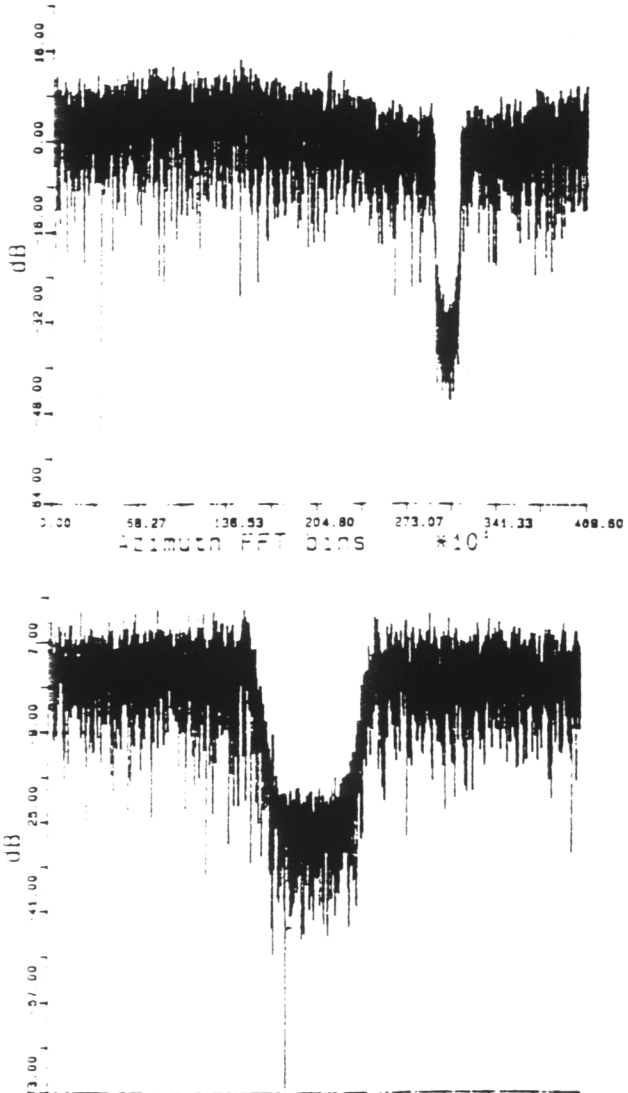

Fig. 2. Range (a) and azimuth (b) spectra of the VMP-SLC product over the point targets zone.

Sadly, only three calibrators are clearly visible and well defined against the background, and they are expected to have a suitable SNR for our purposes. These point targets have been identified as Corner Reflectors Nos. 3 and 7, and ARC No. 2. In Fig. 3, a three-dimensional plot of the image of the ARC is shown, with the z-axis representing amplitudes in arbitrary units (uncalibrated image).

With an oversampling factor M_0=64, we have obtained 2048 complex values in the range and azimuth lines containing the point target No. 2 (ARC). Figures 4a and 4b show the range and azimuth responses.

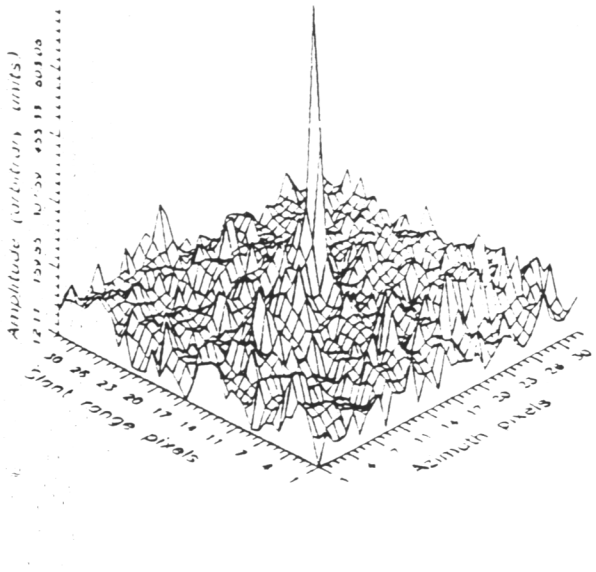

Fig. 3. Pixel values on the 32-by-32 pixel box surrounding point target no. 2 (ARC).

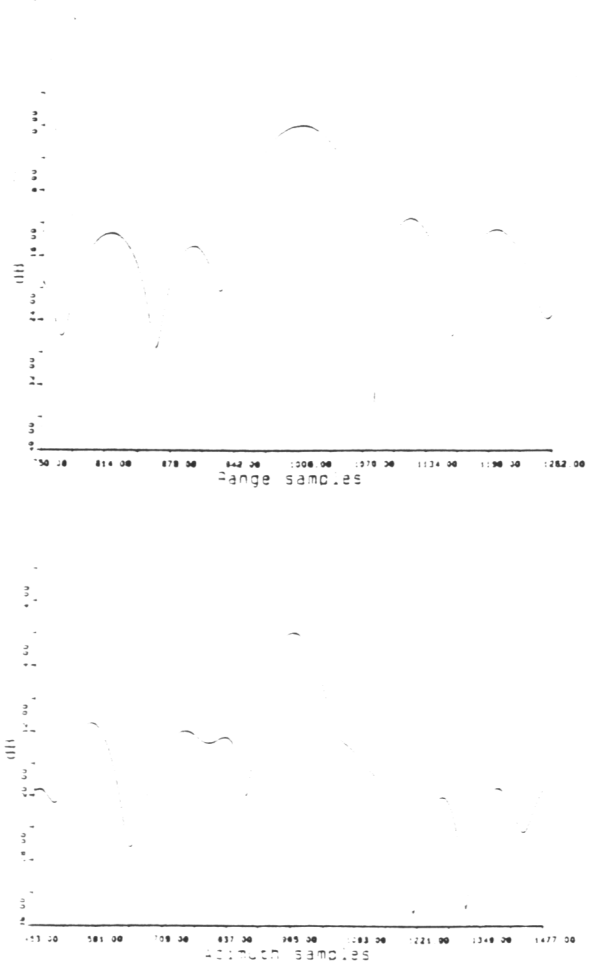

Fig. 4.Active Radar Calibrator (ARC) oversampled response: (a) range, (b) azimuth. Oversampling factor M_0= 64.

The results of the image quality analysis are shown in Table 3, while in Table 4 the mean values and their standard deviations are compared with the nominal ones, giving rise to very small spatial "broadening factors", which indicate a little dispersion of the spatial capabilities of the SAR system due to processor errors. On the other hand, the results on integrated and peak energy measures are not so striking: while in the range direction the energy is still focused in the mainlobe, whith little dispersion in the lateral lobes, in the along-track dimension the sidelobe energy is greater. Furthermore, the PSLR is quite far from the nominal value of -13.2 dB. This could be due to a sampling problem.

Table 3: Image quality parameters for the point targets #3, 7, 2(ARC).

Point target #	3	7	2 (ARC)
r_{gr} [m]	21.5	21.8	22.9
r_{sr} [m]	8.40	8.52	8.91
$ISLR_r$ [dB]	-4.34	-3.79	-8.52
$PSLR_r$ [dB]	-8.67	-8.52	-11.5
r_{az} [m]	4.88	4.00	4.88
$ISLR_{az}$ [dB]	-3.90	-0.50	-4.67
$PSLR_{az}$ [dB]	-7.23	-3.72	-12.8

Table 4: Statistical analysis of resolutions.

	Measured	Nominal	Broadening factor
r_{gr}	22.08 ± 0.74 m	21.8 m	1.4%
r_{sr}	8.61 ± 0.27 m	8.51 m	1.2%
r_{az}	4.53 ± 0.61 m	4.40 m	4.3%

1.3 I-PAF PRI product

We have analyzed two PRI images provided by the I-PAF processor. The images are related to the October 23, 1991 and the July 7, 1992 data takes, respectively over Taranto area (orbit 1416; frame 801; night pass) and Matera area (orbit 5105; frame 2781; day pass). The PRI product is the result of the processing with 3 looks in azimuth and ground range projection; besides, a Hamming windowing is applied in both azimuth and range directions. This latter modifies heavily the sinc-like shaped impulse response.

The data quality measurements have been performed on the ARC responses after pixel oversampling of M_0=8 by means of FFT technique. As an example of processor performance, in Figs 5a and 5b the azimuth and range cuts of an ARC are drawn. As can be seen, the impulse response with its side lobes structure is well shaped and is symmetrical with respect to the peak response. Table 5 reports the results of measurements about the focusing properties of the processor.

Tab. 5: PRI products I-PAFprocessing. Point target characterization.

DATE	OCT 23 1991		JULY 7 1992	
ARC#	1 (α=21.32°)	2 (α=20.64°)	1 (α=23.82°)	2 (α=23.90°)
ρ_a (m)	25.12	24.96	24.42	25.79
ρ_r (m)	30.32	30.42	28.69	28.90
$ISLR_{10}$ (dB)	-12.029	-14.540	-13.089	-13.653
$ISLR_{20}$ (dB)	-6.290	-8.713	-7.977	-8.057
$PSLR_r$ (dB)	-21.291	-23.364	-21.316	-21.464
$PSLR_a$ (dB)	-18.434	-18.716	-18.942	-19.292

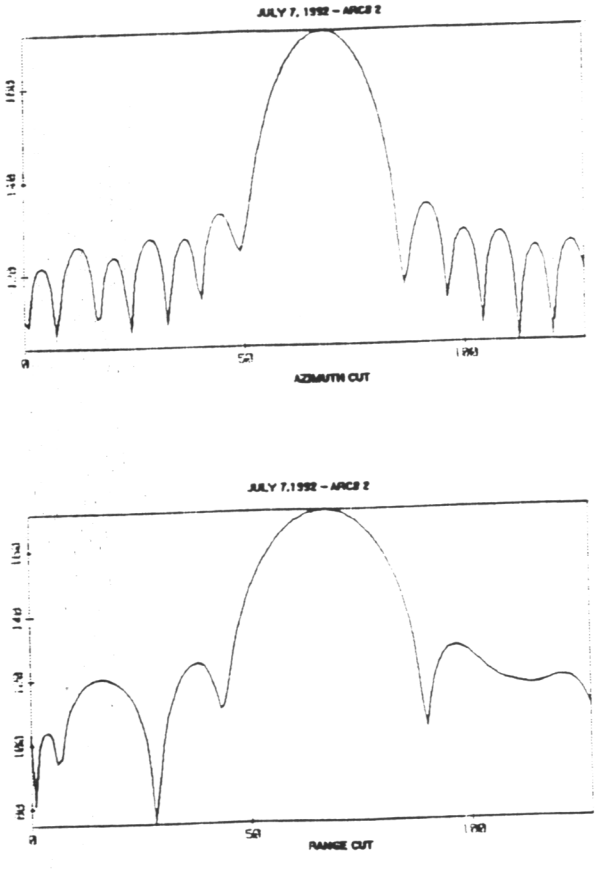

Fig. 5. July 7, 1992 - ARC# 2. (a) Azimuth Cut (b) Range cut.

The resolution values found and the ISLR and the PSLR as well, are within the expected ones. In fact, the azimuth resolution is less than 26m in both dates, 30m is the allowed ESA's upper bound, and the range resolution is also well within the ESA 33m specification. Taking into account the background contribution, ISLR and PSLR values are also in good agreement with the expected ones. These results confirm the qualitative evaluations of good focusing made after the impulse response function visual inspection.

1.4 Data quality analysis on ω-k processor

Within our group, a ω-k processor is available whose capability has been tested for data from the ERS-1 platform related to the October 23, 1991 acquisition. Although the results presented herein are preliminary, they are encouraging for the continuation of our experiment. Raw data have been processed in single look, slant range format without data windowing. Fig. 6 is the bidimensional representation of the impulse response function from an ARC after M_0=2 oversampling, range and azimuth cuts have been extracted and plotted in Figs 7a, 7b.

Table 6: Image quality parameters as a result of the ω -k processor.

ARC#	1	2
Inc. Angle	21.32	20.64
r_{gr} [m]	24.4	24.6
r_{sr} [m]	8.8	8.7
$ISLR_r$ [dB]	-9.07	-9.48
$PSLR_r$ [dB]	-13.64	-13.43
r_{az} [m]	7.3	4.0
$ISLR_{az}$ [dB]	-10.14	-8.44
$PSLR_{az}$ [dB]	-14.82	-10.24

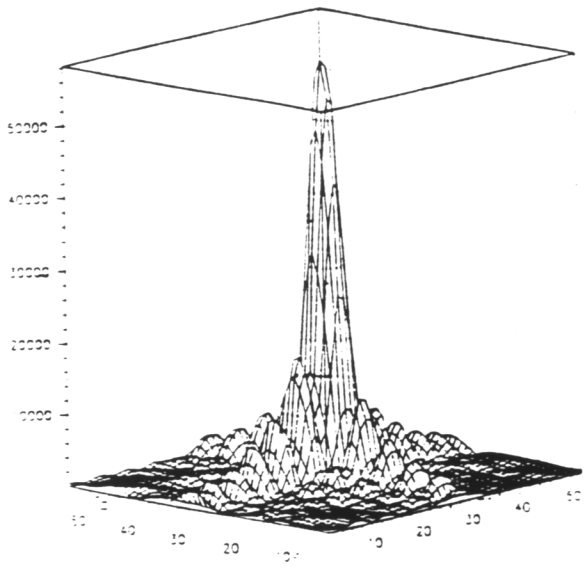

Fig. 6. IRF of ARC# 1 - ω - κ processing.

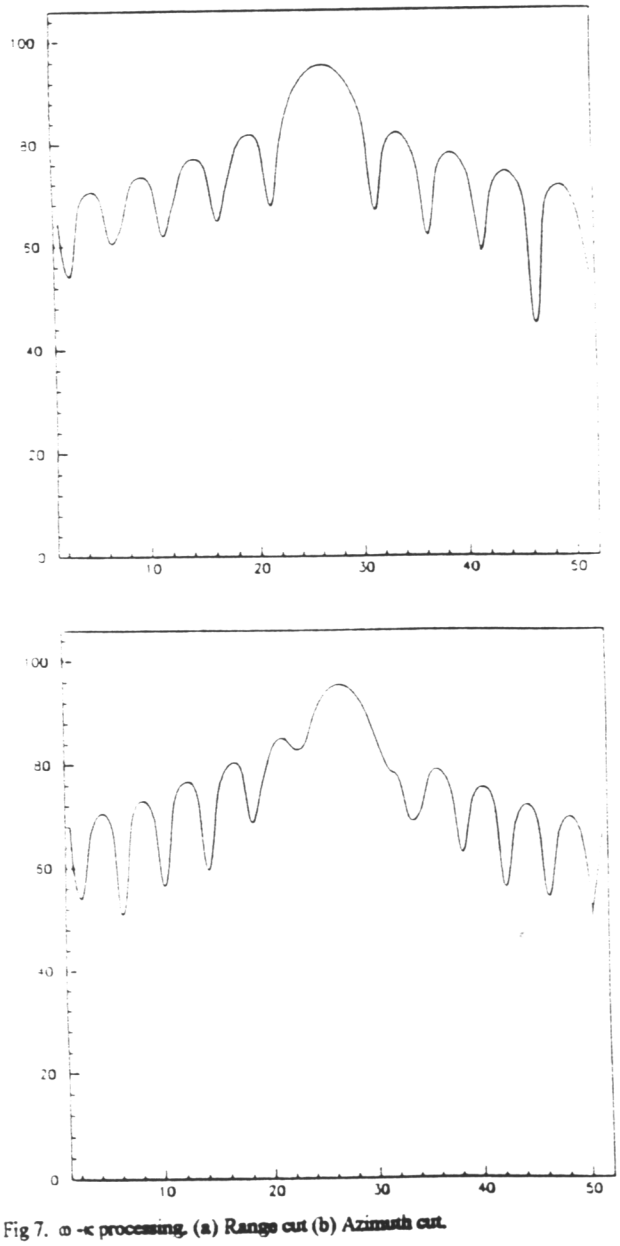

Fig 7. ω -κ processing. (a) Range cut (b) Azimuth cut.

The expected sinc-like shaped response is evident from the plots and from the values listed in Table 6. In fact, the resolutions are well within those expected, as computed from the ERS-1 acquisition set up. Only the ARC 2 azimuth resolution value is quite large, probably due to some clutter effect. The remaining parameters agree very well with those related to a sinc-like response.

2. RADIOMETRIC CALIBRATION

2.1 Background

To avoid biased measurements, the used radiometric calibration strategy is based on the point target integral SAR energy estimation (Ref. 8). Thus, results can be considered both independent of focusing errors and unbiased with respect to those parameters which are related to the imaging geometry (Ref. 4). Actually, calibration measurements carried out by means of the peak method could suffer these problems if the whole chain of data acquisition-processing is only approximately known.

The radiometric analysis has been carried out on the I-PAF PRI product and on the VMP one. The analysis on the PRI images has been aimed at measuring the overall calibration constant of the processor in different dates. This has allowed us to test the radiometric performance of the ARCs deployed on the sites. On the other hand, σ_0 measurements of homogeneous areas embedding the calibrators have been carried out on the VMP product. This to test the reliability of the calibration strategy on single look images.

2.2 Calibration of I-PAF PRI product

In order to better assess radiometry, the ESA transponder responses of the October 13, 1991 Flevoland area acquisition (orbit 1273; frame 1056) after the I-PAF PRI processing have also been considered. In fact, previous ESA measurements aimed at establishing the RCS of each transponder have been used for our purpose.

According to the ESA's criteria, a tile of 4 times interpolated 51×51 pixels was extracted around the peak location of each calibrator. The point target energy estimation has been carried out on a subtile of 31×31 pixels from the previous setting and centered around the peak; the remaining pixels have been used for the estimation of the background clutter which affects the calibrator's response. We have verified that this choice is satisfactory regardless the imaging incidence angle of our calibrators. For all the available point targets, in fact, the whole energy is contained inside the 31×31 frame and the number of pixels used to

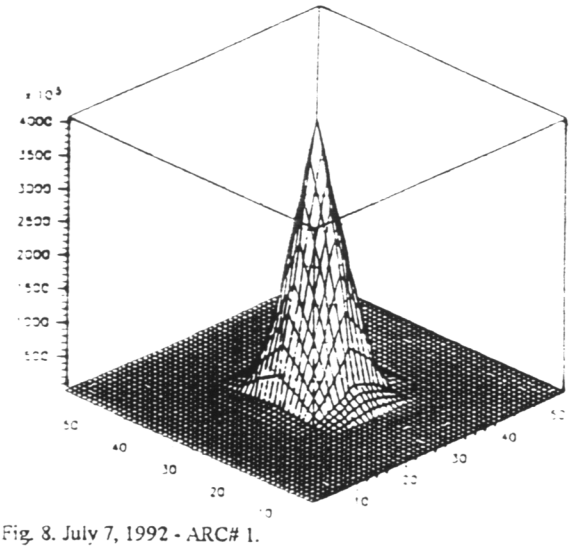

Fig. 8. July 7, 1992 - ARC# 1.

estimate clutter contribution is large enough to give a reliable result. This can be seen in the plot of Fig.8 which is an example of power response from an ARC.

As first step, the calibration constant K for the I-PAF PRI product has been computed from the 3 ESA transponders response deployed on the Flevoland site. The results are reported in Table 7 and refer to the incidence angle α=23°.

Table 7: I-PAF calibration constant K (α=23°) measured on Flevoland image.

Trans #	RCS * (dB)	K (lin)	K (dB)	L bound	U bound
1	58.27 ± 0.40	878415	59.44	740798	1041597
2	57.65 ± 0.40	791425	58.98	665901	940610
3	57.86 ± 0.40	804822	59.06	675616	958738
<K> = 59.16 ± 0.40 (dB)					

* Valid before March 1992

The listed RCS values and 1σ bounds for each transponder are valid for the period ranging from September 1991 until March 1992. A total range of ≈0.5 dB is found for K, while a standard deviation of 0.4 dB can be attributed to the average value (<K>=59.16 dB). These uncertainty ranges do not include the clutter effect because of its negligibilty. Next, the upper and lower bounds in linear units for each K value are given. They take into account the worst cases related to the maximum variation (±0.75 dB) of the measured RCSs. The computed calibration constant <K> has been applied to our data set giving good results for the RCS estimation of the couple of CRs deployed on the Taranto site. This was expected because of the narrow temporal interval between the two data takes. The results are listed in Table 8a. On the other hand, measurements performed on CRs deployed on the Matera site gave results which sistematically overestimate of ≈0.5 dB the expected RCS values (see Table 8b). On this basis, the updated calibration constant has been computed for each CR response and the new value taken as:

$$<K_{new}> = 59.65 \pm 0.30 \text{ dB}$$

Table 8. a and b: Summary of the calibration results.

a) OCTOBER 23 1991

CR#	$\sigma_{(FLEVOLAND)}$	$\sigma_{(EXPECTED)}$	Δ
1	40.78	41.35	-0.57
2	40.43	41.35	-0.92

b) JULY 7 1992

CR#	$\sigma_{(FLEVOLAND)}$	$\sigma_{(EXPECTED)}$	Δ	K_{new}
1	41.95	41.37	+0.58	59.74
2	42.03	41.38	+0.65	59.81
3	42.00	41.39	+0.61	59.77
4	41.47	41.38	+0.09	59.25
K_{new} = 59.65 ± 0.30				

The variation in the K value could be attributed to aging effects which have affected the operation of the ERS-1 on board instrumentations. However, our results should be considered very preliminary because the measurements have been carried out by means of devices whose reliabilty is not completely assessed.

Besides corner reflectors deployment, two ARCs were located in both sites. Their radiometric performance has been checked in order to have a comprenensive knowledge of the whole gain chain which include the receiving and transmitting antennas. At the moment, in fact, the radiometric characterization of the ARCs by means of laboratory measurements is in progress.

Table 9 summarize the calibration results carried out on the ARC responses by means of the calibration constants previously computed.

Table 9: Results of the radiometric analysis from the PRI I-PAF product performed on the ARCs

DATE	OCT 23 1991		JULY 7 1992	
ARC #	1 (α =21.32°)	2 (α =20.64°)	1 (α =23.82°)	2 (α=23.90°)
S/C (dB)	30.16	31.67	31.61	30.10
σ_{exp} (dBm^2)	54.80	56.80	52.00	52.00
σ_{meas} (dBm^2)	56.25	59.51	55.45	54.70
Δ	1.45	2.71	3.45	2.70
k (α=23°) (dB)	59.16 ± 0.40 *		59.65 ± 0.30 **	

* Flevoland; ** Our Measurement

Measurements give biased results of RCS values with respect to the expected ones. These latter are sistematically lower and it seems that ARC#2 have a more stable behaviour than ARC#1 for different environmental conditions. In fact, between the acquisitions a temperature variation of ≈25°C due to the different seasons and the time of the passes was recorded. At the present, we cannot give any further explanation about the experimental observations.

2.3 VMP radiometric analysis

The radiometric calibration approach adopted in the following is essentially described in (Ref. 8), (Ref. 9) where it is shown that $\langle \sigma_0 \rangle$, the spatial averaged estimate of σ_0, is given by:

$$\left\langle \sigma^0 \right\rangle = \frac{\sigma\, \mathcal{E}_{gu}}{A_u \mathcal{E}_{gp}} \sin\alpha$$

where σ is the known RCS of the reference reflector, $\mathcal{E}_{gu}$ is the power associated to the background clutter, $A_u = \delta_{sr}\, \delta_{az} / \sin\alpha$ is the uniform target area, where δ_{sr} and δ_{az} are the slant range and azimuth spacings, respectively, $\mathcal{E}_{gp}$ is the energy of the point target. All the energy contributions in the above equation have been evaluated on the processed image by using the intensity integral method. Considering a 16-by-16 pixel box centred around each imaged scatterer, we have carried out the estimates of the following terms:

$$\mathcal{E}_1 = \mathcal{E}_p + \mathcal{E}_u + \mathcal{E}_n$$

$$\mathcal{E}_2 = \mathcal{E}_u + \mathcal{E}_n$$

where $\mathcal{E}_p$ is the image integrated energy associated to the corner reflector, $\mathcal{E}_u$ is the energy associated to the uniform background, and $\mathcal{E}_n$ is the noise energy. By subtracting $\mathcal{E}_2$ from $\mathcal{E}_1$,we get $\mathcal{E}_p$, and by estimating $\mathcal{E}_n$ it has been possible to evaluate the power contribution due to the background clutter. The residual noise term, $\mathcal{E}_n$, is estimated with chirp off-band measurements (Ref. 10). We estimate $\hat{\sigma}_n$, the power spectral density of the noise, by averaging the periodogram estimates of $\hat{\sigma}_n$ for each spectral range line contained in the pixel-box surrounding the target. In this way, we obtained the mean noise energy per FFT bin, and successively the mean noise power per pixel. Finally, by multiplying by the number of pixels included in the clutter zone, an estimate of $\mathcal{E}_n$ was obtained and the values of $\mathcal{E}_{gu}$ and $\mathcal{E}_{gp}$ were attained. As a check of this method, a direct assessment of noise power has been carried out on "non-target" areas, i.e. areas with little backscattering return. These areas were selected by visual inspection on the processed image, and the obtained values of noise power density are in good agreement with the spectral estimate of $\hat{\sigma}_n$. The radiometric output of this analysis are the values of Signal-to-Noise and Signal-to-Clutter Ratios (SNR, SCR). The former has been evaluated by estimating the energy of the point target with the above described integral method, while the latter has been found as a peak signal to-average clutter ratio. The mean value of 19.1 dB is rather low, indicating a weak predominance of the signal with respect to the background clutter. Finally, we found estimates of σ_0 for the background areas of the scatterers, reported in Table 10.

Table 10: Radiometric analysis results

CR #	3	7	2 (ARC)	Mean ± s.d.
SNR [dB]	16.4	10.5	12.7	13.9 ± 2.3
peak SCR [dB]	20.6	16.9	19.0	19.1 ± 1.5
σ_0 [dB]	-15.6	-11.2	-4.20	-10.3 ± 4.7

3. CONCLUSIONS

The Data Quality Analysis has shown that: the ERS-1 AMI instrument is performing outstandingly; the VMP, I-PAF and ω-k processors can provide users with data well within the specifications. The Radiometric Calibration gives good results when using corner reflectors; higher RCS ARCs give some contradictory results that are under detailed investigation.

4. ACKNOWLEDGMENTS

This work is being carried out under the Italian Space Agency contracts: ASI-91-RS-70 and ASI-91-RS-63. We would also to thank Dr. M. Pernioia of the Universita della Basilicata for collecting most of the ground truth data.

5. REFERENCES

1. Cafforio C., Prati C. & Rocca F. 1991, A SAR data focusing using seismic migration techniques, IEEE Trans. Aero., 27, 2, 194-207.

2. JPL SIR-C Team, DLR NE-HF X-SAR Team, I-PAF X-SAR Team 1990, Data Products And Image Quality Specifications For The SIR-C/X-SAR Mission, JPL D-7193.

3. Harris J. E., Ostler R. S., Chambries D. M. & Christiansen R. W. 1988, Quality Measures for SAR Images, Proc. ICASSP, 1064-1067.

4. Raney R. K. 1991, Considerations for SAR Quantification Unique to orbital Systems, IEEE Transactions on Geoscience and Remote Sensing, GE-29, 5, 754-760.

5. Moccia A., Vetrella S. & Ponte S. 1991, Passive and Active Calibrators Characterization by Using a Spaceborne SAR System Simulator, Proc. of the SAR Calibration Workshop, Oberpfaffenhofen, Germany, publ. by DLR.

6. Raney R. K. 1986, Doppler Properties of Radars in Circular Orbits, International Journal of Remote Sensing, 7, 9, 1153-1162.

7. ESA EPO, ERS-1 1992, Fringe Complex Image Data Format.

8. Ulander L. M. H. 1990, Theory of SAR Radiometric Calibration, Dept. Radio and Space Science, Chalmers University of Technology, Göteborg, Sweden, Research Report No. 167.

9. Gray A.L., Vachon P. W., Livingstone C. E. & Lukowski T. I. 1990, Synthetic Aperture Radar Calibration Using Reference Reflectors, IEEE Trans. on Geoscience and Rem. Sens., GE-31, 3, 374-383.

10. CEOS SAR-CAL-VAL Working Group 1991, White Paper on SAR Image Quality Definitions, presented at the SAR Calibration Workshop, Oberpfaffenhofen, Germany, publ. by DLR.